Saber, S.; Mollar García, MA.; El Nahrawy, A.; Khattab, N.; Eid, A.; Abo Ali, M.; Marí, B. (2018). Annealing study of electrodeposited CuInSe2 and CuInS2 thin films. Optical and Quantum Electronics. 50(6). https://doi.org/10.1007/s11082-018-1521-1

Opt Quant Electron (2018) 50:248
https://doi.org/10.1007/s11082-018-1521-1

Annealing study of electrodeposited $CuInSe_2$ and $CuInS_2$ thin films

Suzan Saber[1,2,3], Miguel Mollar[1], Amany El Nahrawy[2], Nagwa Khattab[2], Ali Eid[2], Mohamed Abo-Aly[3], Bernabé Marí[1]

[1] Institut de Disseny i Fabricació, Universitat Politècnica de València. Camí de Vera s/n 46022 València (SPAIN)

[2]National Research Center, 33 El Bohouth St. (former El Tahrir St.) - Dokki - Giza - Cairo (EGYPT)

[3]Chemistry Department, Faculty of Science, Ain Shams University, Cairo (EGYPT)

Abstract:

In this study $CuInSe_2$ and $CuInS_2$ thin films were prepared onto ITO glass substrate using the electrodeposition technique in aqueous solution. The electrodeposited films were characterized by X-ray diffraction (XRD), scanning electron microscopy (SEM) and energy dispersive X-ray analysis (EDS). The annealing effects on electrodeposited precursors were investigated. The chalcopyrite structure of $CuInSe_2$/$CuInS_2$ showed an enhancement of crystallinity after subsequent selenization/sulfurization treatment in Se/S atmosphere, respectively. XRD and SEM studies revealed a dramatic improvement of the crystalline quality of CIS films after annealing treatments. Mott-Schottky measurements were used to assess the conductivity type of the films and their carrier concentration. The prepared samples underwent an etching process to remove the binary accumulated $Cu_{2-x}(Se,S)$ phases shown in FESEM pictures. This etching process has shown a noticeable decrease in both, the flat band potencial, V_{fb} *(V),* and the number of acceptors, N_A *(cm^{-3})* in selenized $CuInSe_2$ and sulfurized $CuInS_2$ samples.

Keywords:

$CuInSe_2$; $CuInS_2$; Electrodeposition; Mott-Schottky; Solar Cells.

1. Introduction

Many years ago the gradual and unavoidable consumption of natural energy sources like fossil fuels lead to massive demand of energy alternative sources all over the world [1]. In addition, to solve the problems related to heating and greenhouse effect, it's important to take in consideration those of renewable energy sources, e.g., solar, hydro, wind, tidal, ocean, and geo-thermal energy. One of these renewable energy sources is photovoltacis (PV) technology. This is a widespread alternative source as their low cost and effectiveness choice. It depends on charge carrier generation in some type of light sensitive materials. The first applied solar cell was proposed by Grätzel in 1991 [2]. Among those (PV) technologies thin-film semiconductor absorber materials. In this type of thin-films sunlight is converted directly into electricity, Such as CdTe, CdSe, PbS, $CuInSe_2$, $CuInS_2$, $CuIn(Se,S)_2$, $CuInxGa_{1-x}Se_2$ and $Cu(In,Ga)(Se,S)_2$ [3].

$CuInSe_2$ is considered a benign absorber material for thin-film solar cells, due to its high absorption coefficient of about 10^5 cm^{-1} and its band gap nearly 1.5 eV with a well match to the solar spectrum. In addition, $CuInS_2$ is low-cost, environmentally friendly material, and has a long-term stability in photovoltaic applications [4]. Electrodeposition-based technique is one of the foremost promising approaches to reach an enhanced reduction in the production cost this thin film types. Due to its low-temperature processing, large area deposition, and negligible waste of chemicals with higher efficiencies close to100%. Therefore, several research groups have studied fabrication of $CuInSe_2$, $CuIn(Se,S)_2$, and CIGS-based solar cells by electrodeposition [5]. So, several techniques have been developed to prepare CISSe thin film solar cells such as, mechanical milling [6], chemical bath deposition [7], evaporation [9], paste coating technologies [11], magnetron sputtering [11], microwave irradiation [12,13] and solvothermal method [14], electrodeposition [15], in order to improve their efficiencies. Some of these methods, in particular the chemical-based ones, have the advantages of simplicity, high throughput and inherent low investment requirements.

Hence, in the present study, we prepared $CuInSe_2$ and $CuInS_2$ thin films from previously electrodeposited $CuInSe_2$ films by selenization or sulfurization of in an Se or S-rich atmosphere, respectively, in a graphite box under N_2+H_2 gas in a quartz tube vacuum oven. Then, we further investigated the effect of precursors on the properties of CIS films by X-ray diffraction (XRD), scanning electron microscopy (FESEM) and Mott-Schottky measurements.

The use of Schottky barrier solar cells based on thin-film semiconductors is another way to improve solar cell performance. The Mott-Schottky plot is a usual way for semiconductor material

electrochemical characterization [16-18]. A Mott-Schottky plot (inverse square of space charge layer capacitance (C_{sc}^{-2}) versus semiconductor electrode potential (E) gives the doping density by slope of the straight line and flat-band potential by x-axis intercept.

Theory of CIS electrodeposition:

$CuInSe_2$ thin film electrodeposition conditions were first introduced by Bhattacharya (1983) [19]. This is by far the most investigated such a process, usually referred to as single-step electrodeposition; it involves only one electrochemical process. The drawbacks of this process is that the electrochemical features is arbitrarily difficult control, either the formation of the elements in their elemental form, or as binary compounds additionally to the required ternary CIGS chalcopyrite phase, that refers to the fundamental individual electrochemical reactions concerning the deposition of Cu, In and Se [20]. The single-step electrodeposition of CIS from aqueous solution containing $CuCl_2$, $InCl_3$, and H_2SeO_3 according to the Nernst equation is quite difficult and difference in the reduction potential between these ion species is rather large. The electrochemical reduction reactions among Cu, In and Se ions is illustrated in the following equations [21] (vs. NHE, normal hydrogen electrode):

$$Cu^{2+}{}_{(aq)} + 2e^- \rightarrow Cu_{(s)} \quad \text{----------} \quad (1)$$

$$E = E^0 - \frac{RT}{2F} \cdot \ln\left(\frac{a_{Cu}}{a_{Cu^{2+}}}\right) = 0.342 + 0.0295 \log a_{cu^{2+}} \quad \text{----------} \quad (2)$$

$$In^{3+}{}_{(aq)} + 3e^- \rightarrow In_{(s)} \quad \text{----------} \quad (3)$$

$$E = E^0{}_{In} - \frac{RT}{3F} \cdot \ln\left(\frac{a_{In}}{a_{In^{3+}}}\right) = -0.338 + 0.0197 \log a_{In^{3+}} \quad \text{----------} \quad (4)$$

$$H_2SeO_{3(aq)} = HSeO_2 + (aq) + OH^-{}_{(aq)} \quad \text{----------} \quad (5)$$

$$HSeO_2 + (aq) + 3H^+{}_{(aq)} + 4e^- \rightarrow Se_s + 2H_2O_{(l)} \quad \text{----------} \quad (6)$$

$$E = E^0{}_{Se} - \frac{RT}{4F} \cdot \ln\left(\frac{a_{Se}}{a_{HSeO}}\right) + 2\, a_{3H^+} = 0.74 + 0.0148 \log a_{HSeO^{2+}} - 0.043\, pH \quad \text{--------} \quad (7)$$

where E refers to the deposition potential of Cu, In, and Se, R is the ideal gas constant, F is the Faraday constant, a_X, where (X=Cu,Cu^{2+},In, In^{3+}, Se, $HSeO^{2+}$ and H^+)refer to activities of Cu, Cu^{2+}, In, In^{3+}, Se, $HSeO_2^+$, and H^+, respectively. To manage a good deposition process, some complexing agents were used in order to bring deposition potentials of the ion species closer by shifting the copper ion potential into the negative direction.

2. Experimental Procedure

2.1. Thin film preparation

$CuInSe_2$ (CIS) films were electrodeposited using Indium-doped tin oxide (ITO) as substrates. Before deposition process, substrates were cleaned successively in an ultrasonic bath with detergent, alcohol solution, and acetone then rinsed with deionized water and subsequently dried. A three-electrode cell was used with a Pt wire as a counter electrode, a (Ag/AgCl) as reference electrode, and the working electrode was ITO coated glass substrate. Electrodeposition was carried out employing an Autolab PGSTAT 302N. The electrolytic bath was consisting of an acidic aqueous solution containing 0.025 mol/L $CuCl_2$, 0.025 mol/L $InCl_3$, and 0.025 mol/L H_2SeO_3 dissolved in high-purity distilled water. The pH of the electrodeposition bath was adjusted at 1.5 using hydrochloric acid (HCl). Also, the addition of KCl as supporting electrolyte provides better stability of the electrodeposition bath solution and improves the quality of the deposited layers. CIS thin films were electrodeposited in potentiostatically, applying a potential of -0.90V vs. Ag/ AgCl for 30 min. Before deposition, the solution was deaerated by argon bubbling and stirred up for 20 min. After completing the electrodeposition the samples were rinsed with distilled water and dried in air. Then, the as-deposited $CuInSe_2$ films were annealed at 450°C for 20 min under nydron forming gas (10 % H_2 in N_2) atmosphere with a pressure of 10^{-2} bar to improve the crystallinity of the resulted films. A sulfurization process was performed onto the electrodeposited $CuInSe_2$ layers to obtain $CuInS_2$ films. A sufficient amount of molecular sulfur was loaded into a graphite box inside a quartz tube under the forming gas atmosphere. The oven temperature was kept at 400°C for 10 min. Form now on, the selenized $CuInSe_2$ samples will be referred as $CuInSe_2$-Se and the sulfurized $CuInSe_2$ samples will be referred as $CuInSe_2$-S.

2.2. Characterization

The crystal structure of $CuInSe_2$ as grown, $CuInSe_2$-Se selenized and $CuInSe_2$-S sulfurized thin films was investigated using X-ray diffraction (XRD) Rigaku Ultima IV diffractometer with the Bragg-Bentano configuration and CuKα radiation (λ = 1.54060 Å). Chemical composition, surface morphology and topography were characterized using energy dispersive spectroscopy (EDX) and field emission scanning electron microscopy (FESEM).

Mott-Schottky measurements were applied to investigate the manner of the prepared semiconductor layers. Mott-Schottky studies were employed using 0.5 M NaOH as an electrolyte

in a three-electrode electrochemical. Reference Ag/AgCl electrode was used and a platinum wire as a counter electrode. Working electrodes were prepared using ITO n-type and $CuInSe_2$-Se $CuInSe_2$-S p-type thin films. The ohmic contacts were made using copper wire and a conductive silver paste. The nature of those ohmic contacts was tested before measurements. The relevant measured area of the photo-electrodes was 0.32 cm^2.

3. Results and discussion

3.1. XRD analysis

Fig. 1 shows the XRD pattern of the prepared samples containing three diffraction peaks. The first one is for the as-grown $CuInSe_2$ electrodeposited thin films. The second is for the selenized samples and the rest is for the sulfurized samples. The diffraction pattern of the as-grown $CuInSe_2$ polycrystalline thin films evidences poor crystallinity. The as-grown electrodeposited sample shows broad peaks with a low intensity at the positions (112, 220/204 and 116/312) indicating that the grown films have to be annealed for good crystallinity. Also, characteristic peaks with higher intensity for the ITO substrate, marked with *, are obviously shown. The tetragonal structure of the $CuInSe_2$ deposited onto ITO was observed with very small particle size 6 nm. After the annealing processes with selenium (selenization) and sulfur (sulfurization) both in inert atmosphere using Nydron gas (10% of H_2 in N_2), the crystallinity of the prepared samples improved, i.e., the characteristic peak intensity of both $CuInSe_2$ and $CuInS_2$ increased give the improved crystallinity of the prepared samples. The peak position shifts considerably to higher 2θ angles for the sulfurized samples. For the selenized samples the resulted crystallite size was 61 nm. The peaks of $CuInSe_2$ situated at 2θ=26.68, 44.38 and 52.63 degree for 112, (204/220) and (116/312) diffraction planes, respectively, match those of the JCPDS-040-1487 of the $CuInSe_2$ reference card. The diffraction peaks of sulfurized samples were clearly obtained at 27.86, 46.31 and 54.82 degree for 112, (204/220) and (116/312) diffraction planes, respectively, matching those of the JCPDS-027-0159 $CuInSe_2$ reference card with a crystal size of 34 nm calculated at 112 main peak as shown in Table 1.

Opt Quant Electron (2018) 50:248
https://doi.org/10.1007/s11082-018-1521-1

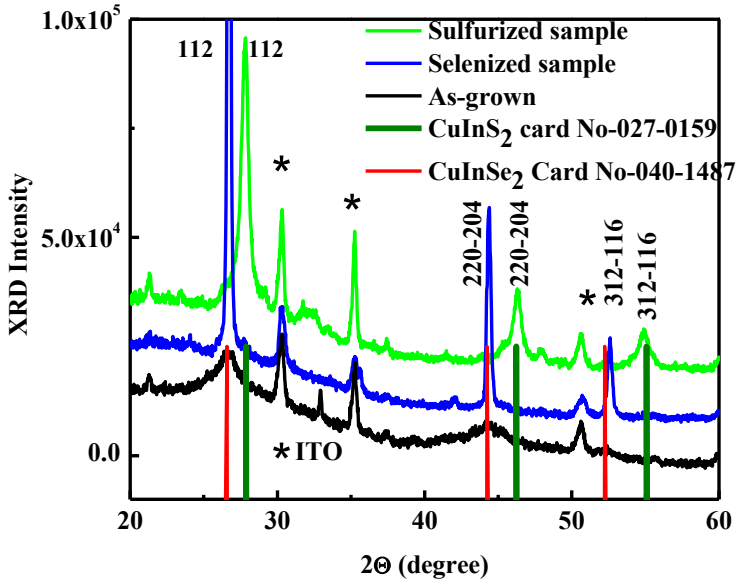

Fig. 1. XRD spectra of $CuInSe_2$ as-grown, sulfurized and selenized films.

The crystallite size of the prepared films was calculated according to Scherer's formula:

$$D = \frac{K\lambda}{\beta cos\theta} \qquad (8)$$

where β is the Full Width at Half Maximum (FWHM), λ wavelength of X-rays with value is 1.5418 Å, K is Scherer's constant depending on the crystallite shape and is close to 1 (K= 0.9 was used) and θ is the Bragg angle at the center of the peak.

Table 1. Crystallite size measurement of $CuInSe_2$ as-grown, sulfurized and selinized films.

Sample	Crystallite size (nm)
As grown $CuInSe_2$ ($CuInSe_2$)	6
Sulfurized $CuInSe_2$ ($CuInSe_2$-S)	34
Selenized $CuInSe_2$ ($CuInSe_2$-Se)	61

Table 1 displays the crystallite size of different studied samples calculated through the Sherrer equation. The crystallite size of the as grown samples, with molecular formula $CuInSe_2$, is about 6nm. Independent of the gas used, the subsequent annealing produces an effective increase of the crystallite size. In sulfur atmosphere, sulfur atoms replaced most of selenium atoms forming $CuInS_2$ phase. With the smaller atomic size of sulfur than selenium and the growing up of the grains together the calculated crystal size is about 34 nm, which is more than five times larger than

that measured for the as grown films. Annealing in selenium atmosphere still produces larger crystallites and the growing up process of the selenized phase $CuInSe_2$ in selenium rich atmosphere leads to an increase in the crystallite size up to 61 nm. This can be due to the fact that selenium atoms are larger than sulfur atoms, the higher temperature processed for annealing in case of selenium and the time of annealing.

3.2. FE-SEM analysis

Figure 2 shows FE-SEM images for the $CuInSe_2$-Se and $CuInSe_2$-S films at different magnification scale. It can be clearly seen that all films were uniform, homogenous, well-covered with good adherence. An agglomeration of grains in the films and some $In_2(Se,S)_3$ and $Cu_{2-x}Se$ hexagonal secondary phases in both $CuInSe_2$-Se and $CuInSe_2$-S films can be seen.

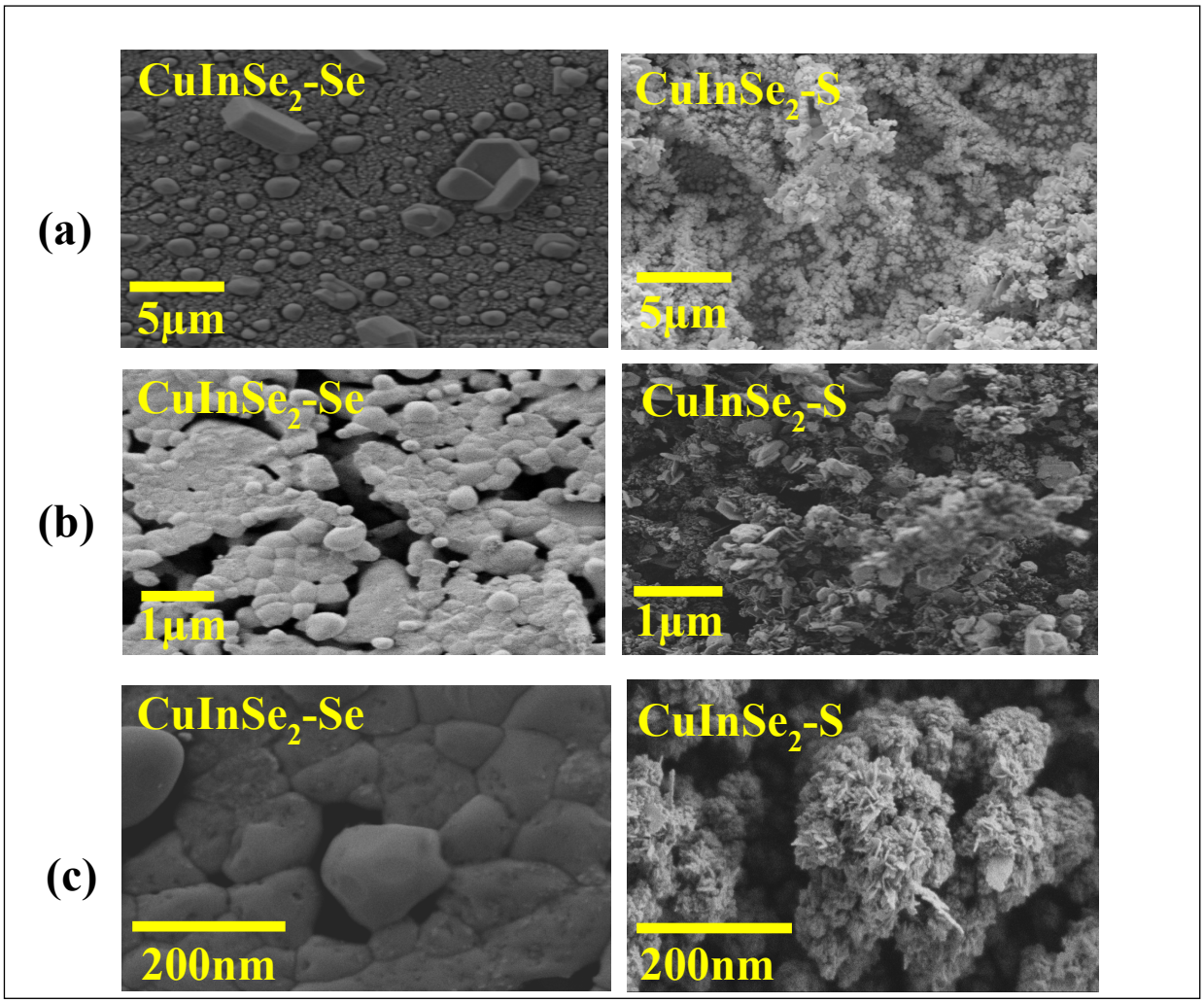

Figure 2. FE-SEM images for ($CuInSe_2$-Se) selenized and ($CuInSe_2$-S) sulfurized films at different magnification scales (a) 2µm, (b)1µm, (c)200nm.

According to the EDX measurements, the selenized and sulfurized $CuInSe_2$-Se and $CuInSe_2$-S films contained 24.86, 23.92 at.% Cu, 27.49, 33.07 at.% In, 47.65, 2.28 at.% Se and, 38.0 at.% S, respectively, corresponding to copper poor $CuInSe_2$-Se and $CuInSe_2$-S phases with an optimum Cu/In ratio of 0.9 and 0.7 for p-type semiconducting properties [20]. Table 2 displays the EDX results for these samples.

Table 2. Composition of the $CuInSe_2$-Se and $CuInSe_2$-S films measured by EDS.

Sample	Cu (at%)	In (at%)	Se (at%)	S (at%)	(Cu/In)	(Se&Se+S)/(Cu+In)
$CuInSe_2$-Se	24.86	27.49	47.65	-----	0.9	0.9
$CuInSe_2$-S	23.92	33.07	2.28	38.00	0.7	0.7

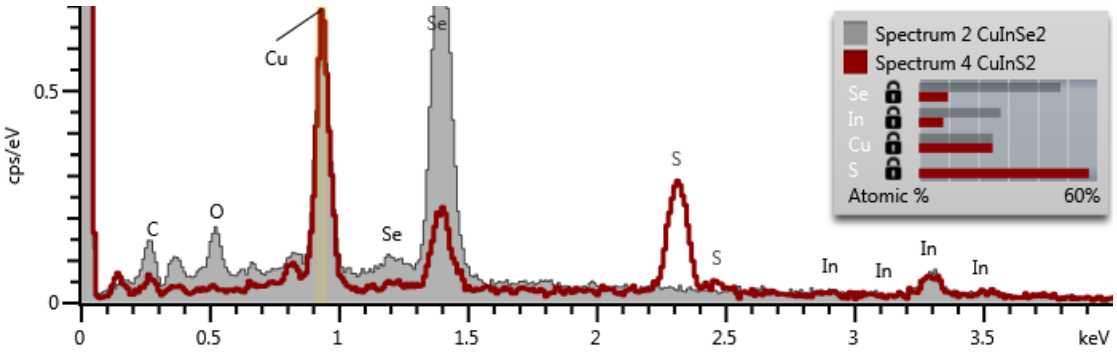

Fig.3. EDX spectrum for both $CuInSe_2$ selenized and $CuInS_2$ sulfurized samples.

3.3. Optical measurements

The optical properties of annealed $CuInSe_2$-Se and $CuInSe_2$-S thin films have been studied in order to determine the effect of annealing process in different selenium and sulfur atmosphere. The optical transmittance spectra were measured in the wavelength range 400 - 1000 nm of the visible region.

Figure 4 show the transmitance spectra of $CuInSe_2$ samples annealed in Selenium and Sulfur atmosphere, respectively. The optical properties are studied, the transmission spectra of the sample $T(\lambda)$ are measured:

Opt Quant Electron (2018) 50:248
https://doi.org/10.1007/s11082-018-1521-1

$$T(\lambda) = \frac{I(\lambda)}{I_0(\lambda)} \qquad (9)$$

where $I_o(\lambda)$ is the intensity of light illuminating the sample, $I(\lambda)$ is the intensity of the light transmitted through the sample. Often one uses the term absorbance (or optical density), which is defined according to the formula (10):

$$\text{Abs}(\lambda) = \log\left\{\frac{I_0(\lambda)}{I(\lambda)}\right\} = -\log\left(T(\lambda)\right) \qquad (10)$$

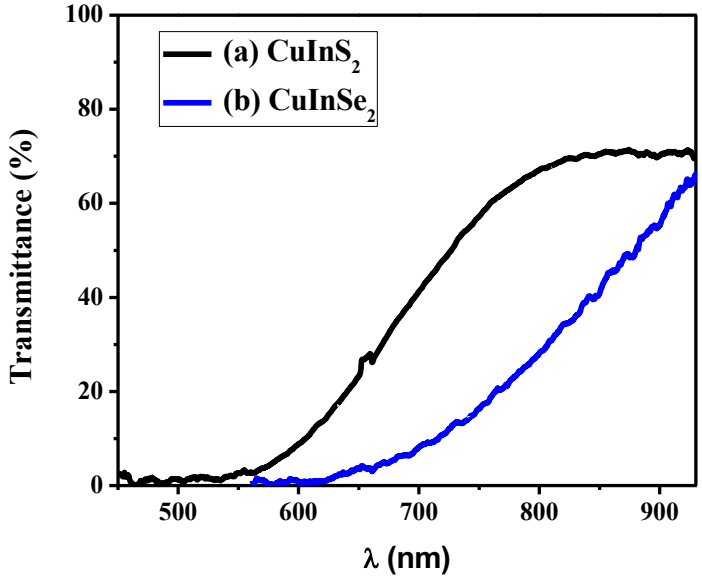

Figure 4. Transmitance spectra of $CuInSe_2$ samples annealed in Selenium and Sulfur atmosphere.

The bandgap energy was determined from the Tauc relationship, Eq. (11):

$$(\alpha h\upsilon) = A(h\upsilon - Eg)^n \qquad (11)$$

Where A is constant, hυ is the photon energy of the incident radiation, Eg is the band gap energy, n=½ for allowed direct transition and n=2 for allowed indirect transition.

As $CuInSe_2$-Se and $CuInSe_2$-S is a direct allowed band transitions, so n=1/2.

$$(\alpha h\upsilon) = A(h\upsilon - Eg)^{1/2} \qquad (12)$$

By square the values of both sides we will got that:

$$(\alpha h\upsilon)^2 = A(h\upsilon - Eg) \qquad (13)$$

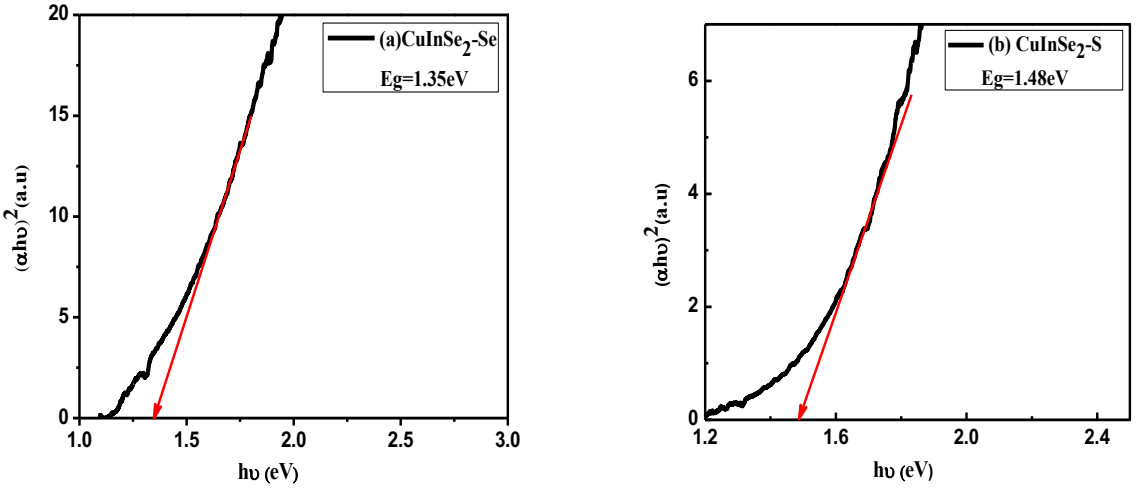

Fig. 5. Tauc plots for (a) selenized $CuInSe_2$ –Se and (b) sulfurized $CuInSe_2$ –S thin films.

Figure 5 (a, b) shows plotting the values of $(\alpha h\upsilon)^2$ as a function of photon energy ($h\upsilon$) for $CuInSe_2$-Se and $CuInSe_2$-S, respectively. The band gap values can be obtained by extrapolating the slope of curves to the X-axis where $(\alpha h\upsilon)^2 = 0$.

The optical band gap is found to be 1.48 and 1.35 eV, for $CuInSe_2$-Se and $CuInSe_2$-S which is agreement with the reported values of the optical band gap of $CuInSe_2$ and $CuInS_2$ [22], As we notice the difference in annealing temperatures and time also affects the resultant band gap energy in addition to the Se/S percentages in both samples.

3.4. Mott-Schottky measurements

To study the charge distribution of the prepared thin films capacity/electrode potential has been studied. The capacity/electrode potential is very sensitive to changes in the charge concentration. Applying Mott-Schottky relationship:

$$\frac{1}{C_{sc}^2} = \frac{2}{qNA^2\varepsilon\varepsilon_0}\left(E - E_{fb} - \frac{kT}{q}\right) \qquad (14)$$

where the capacity of space charge is referred as Csc, the carrier density N is (the concentration of electron donor for n-type semi-conductor or hole acceptor for the concentration of p-type semi-conductor), the relative electric permittivity is ε, the electric permittivity of vacuum is ε_0, the electronic charge is q, the surface area is A, the Boltzman constant is k, the absolute temperature T, E_{fb} is the flat band potential and E is the applied potential.

Opt Quant Electron (2018) 50:248
https://doi.org/10.1007/s11082-018-1521-1

By plotting $1/C^2$ vs. V we suspect obtain a straight line with appositive or negative slope. The plot intercept of dC_{sc}^{2-}/dE with the potential axis yields the flat band potential E_{fb}. The flat band potential E_{fb} does not depend on time nor polarization of the layers. The carrier density N can be derived from the gradient dC_{sc}^{2-}/dE, and the intercept with the potential axis yields the flat band potential E_{fb}. Mott-Schottky equation is used for determining the carrier density and the flat band potencial characterizing semiconductor layers [23].

The electrochemical solution used for mott–Schottky measurement was deaerated with argon. The distinguished layer formed by a potentiodynamic cycling in different potential ranges by means of an auto Lab system PGSTAT 302N conducted at 10kHz. The measurements were conducted at room temprature. The calculated negative slope of C_{SC}^{-2} vs. potential is inversely proportional to the acceptor concentration and is an indication of a p-type semiconductor layer. In contrast the positive slope of C_{SC}^{-2} vs. potential refers to an n-type semiconductor.

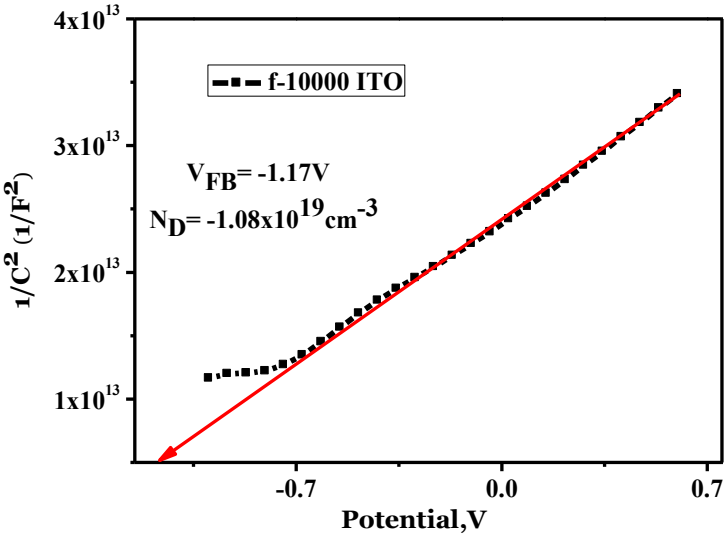

Figure 6. Mott-Schottky plots for n-type ITO.

Opt Quant Electron (2018) 50:248
https://doi.org/10.1007/s11082-018-1521-1

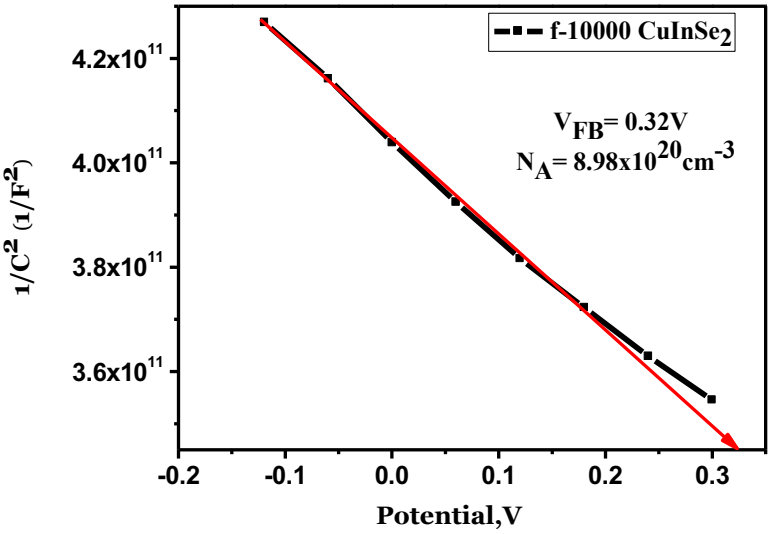

Figure 7. Mott-Schottky plots for p-type $CuInSe_2$ selenized thin films.

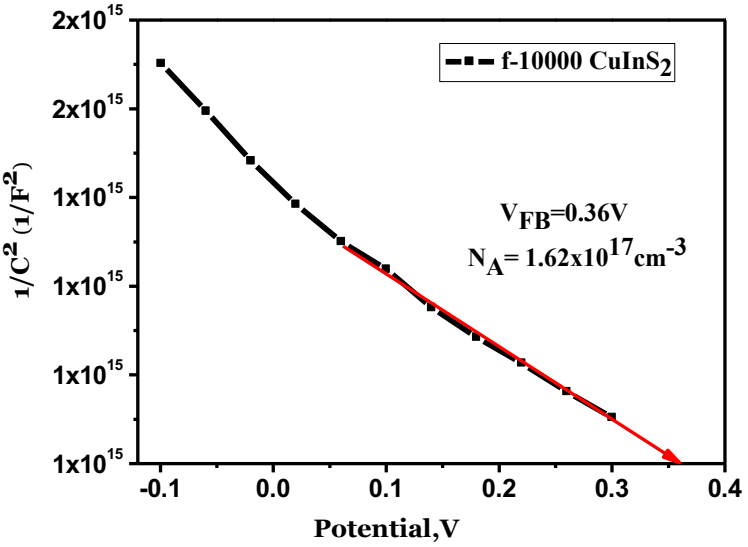

Figure 8. Mott-Schottky plots for p-type $CuInS_2$ sulfurized thin films.

Figures 6, 7, 8 show the plots of Mott-Schottky measurements for ITO and CIS thin-films ($1/C^2$ vs. V) in 0.5M NaOH. Figure 5 shows the Mott-Schottky (MS) plot for the ITO substrate layer. The resulting slope was positive, indicating that the ITO film is an n-type semiconductor. The flat band potential was found to be -1.17V (vs SCE) by extrapolating the linear section to the x-axis and $N_D \approx 1.18 \cdot 10^{19}$ cm^{-3} was measured using the slope of the curve. Figures 6 and 7, respectively, show the plots for $CuInSe_2$-Se selenized and $CuInSe_2$-S sulfurized films. The calculated slopes of the (MS) plots were negative, verifying that the prepared CIS thin film is a p-type semiconductor. The flat band potential was found to be 0.32 and 0.36 V (vs SCE), respectively, extrapolating the linear section to the x-axis. The carrier concentrations, $NA \approx 8.98 \cdot 10^{20}$ and $1.62 \cdot 10^{17}$ cm^{-3}, were calculated using the slope of the curves for both $CuInSe_2$-Se and $CuInSe_2$-S films, respectively. It was noticed that the flat-band potential and acceptor density determined were slightly higher than the p-type semiconductor CIS film values [24, 25].

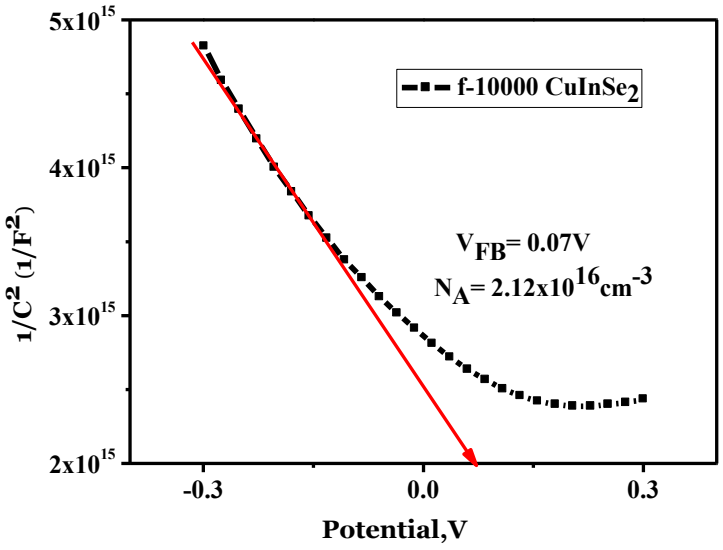

Figure 9. Mott-Schottky plots for p-type etched $CuInSe_2$ selenized thin films.

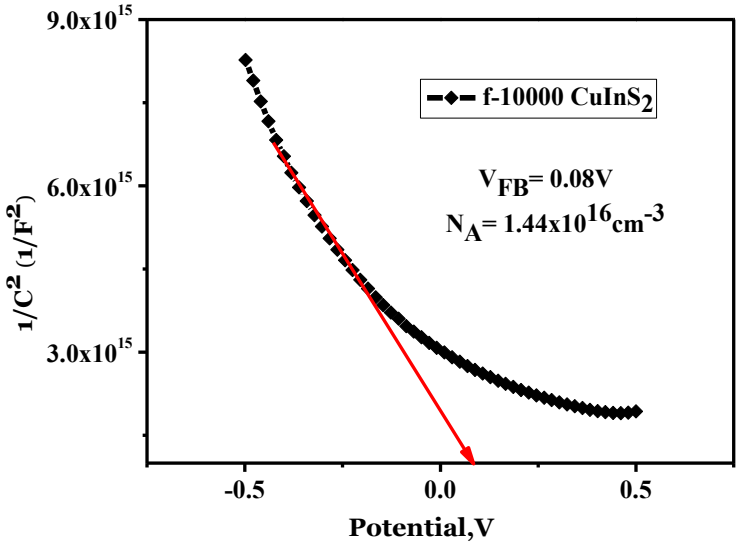

Figure 10. Mott-Schottky plots for p-type etched $CuInS_2$ sulfurized thin films.

Before the etching process, the slope of the Mott–Schottky plots were has a higher doping density $N_A \approx 8.98 \cdot 10^{20}$ and $1.62 \cdot 10^{17}$ cm^{-3} and the x-axis intercept associated with the flat band potential was highly positive 0.32 and 0.36 V (vs SCE). Table 3 displays the flat band potential and number of acceptors of the $CuInSe_2$-Se and $CuInSe_2$-S films before and after etching.

Table 3. Flat band potential Vfb (V) and number of acceptors N_A (cm^{-3}) of the $CuInSe_2$-Se and $CuInSe_2$-S films before and after etching.

Sample Name	Measured values	before etching	after etching
$CuInSe_2$-selenized	N_A (cm^{-3})	$8.98 \cdot 10^{20}$	$2.12 \cdot 10^{16}$
	V_{fb} (V)	0.32	0.07
$CuInS_2$-sulfurized	N_A (cm^{-3})	$1.62 \cdot 10^{17}$	$1.44 \cdot 10^{16}$
	V_{fb} (V)	0.36	0.08

In order to explain the resulting number of acceptor values, an etching process was carried out. Etching process using KCN solution influences the Mott-Schottky results.

Figures 9 and 10 show the Mott-Schottky plots of etched $CuInSe_2$ selenized and etched $CuInS_2$ sulfurized CIS thin-films samples ($1/C^2$ vs. V) in 0.5M NaOH. After the etching process, the slope

of the Mott-Schottky (MS) plots showed a decrease in the doping density, and the calculated carrier density $N_A \approx 2.12 \cdot 10^{16}$ and $1.44 \cdot 10^{16}$ cm^{-3} for etched $CuInSe_2$ selenized and etched $CuInS_2$ sulfurized samples, respectively. Also, a drastic decrease in the flat band potential values was observed. It was found that the flat band potential had decreased to 0.07 and 0.08 V (vs SCE) for etched $CuInSe_2$ selenized and etched $CuInS_2$ sulfurized samples, respectively. The carrier charge density for the etched samples was found to have 10^{17}, 10^{20} to 10^{16} cm^{-3}. This decrease in both N_A and the photocurrent potential was attributed to the etching process. Through etching the accumulation of binary Cu_{2-x}(Se, S) phases shown in FE-SEM pictures was removed. These binary Cu_{2-x} (Se,S) phases are highly conductive, leading to an increase of the flat band potential values. After the etching process the flat band potential is much closer to the literature values for p-type materials, being approximately +0.1 V [24-26]. The shift in the flat band value is due to the change in the position of the Fermi level, which depends on the density of acceptors. After etching, the density of acceptors decreases and then the Fermi level shifts towards the middle of the forbidden band resulting in a drop of the flatband potential (V_{fb}).

5. Conclusion

In this study, a facile methodology for the preparation of p-type $CuInSe_2$ and $CuInS_2$ thin films has been described. The nano-crystalline $CuInSe_2$ and $CuInS_2$ thin films were successfully prepared by a non-vacuum, low cost electrodeposition technique onto ITO substrates. The resulting thin films showed very good crystallinity and homogeneity of the prepared films in agreement with the XRD, SEM and EDX measurements. In order to detect the prepared thin film carrier density type, Mott-Schottky measurements were carried out confirming that the prepared $CuInSe_2$ and $CuInS_2$ thin films were always p-type. The accumulated binary phases of Cu_{2-x}(Se, S) were successfully eliminated through the etching process which in turn decreased both the flat band potential, V_{fb} (V) and the number of acceptors, N_A (cm^{-3}) for the prepared samples.

Acknowledgments

This work was supported by the Culture Affairs and Missions Sector, Ministry of Higher Education and Scientific Research (Egypt) and Ministerio de Economía y Competitividad (ENE2016-77798-C4-2-R) and Generalitat valenciana (Prometeus 2014/044).

References

[1] J.E. Jaffe, A. Zunger, Phys. Rev. B 29 (1984) 1882.
[2] I. Repins, M.A. Contreras, B. Egaas, C. DeHart, J. Scharf, C.L. Perkins, B. To, R. Noufi, Prog. Photovolt. Res. Appl. 16 (2008) 235.
[3] D. Lincot, Thin Sold Films 487 (2005) 40.
[4] I.M. Dharmadasa, N.B. Chaure, G.J. Tolan, A.P. Samantilleke, J. Electrochem. Soc. 154 (6) (2007) H466.
[5] T. Delsol, M.C. Simmonds, I.M. Dharmadasa, Sol. Energy Mater. Sol. Cells 77(2003) 331.
[6] A. Kampman, J. Rechid, A. Raitzig, S. Wulff, M. Mihhailova, R. Thyen, K. Kalberlah, Mater. Res. Soc. Symp. Proc. 763 (2003) 323
[7] R. Friedfeld, R.P. Raffaelle, J.G. Mantovani, Sol. Energy Mater. Sol. Cells 58(1999) 375.
[8] R.N. Bhattacharya, J.F. Hiltner, W. Batchelor, M.A. Contreras, R.N. Noufi, J.R. Sites, Thin Solid Films 361 (2000) 396.
[9] M.E. Calixto, K.D. Dobson, B.E. McCandless, R.W. Birkmire, J. Electrochem. Soc. 153 (6) (2006) G521.
[10] A.M. Hermann, C. Gonzalez, P.A. Ramakrishnan, D. Balzar, N. Popa, P. Rice, C.H. Marshall, J.N. Hilfiker, T. Tiwald, P.J. Sebastian, M.E. Calixto, R.N. Bhattachary, Sol. Energy Mater. Sol. Cells 70 (2001) 345.
[11] S. Taunier, J. Sicx-Kurdi, P.P. Grand, A. Chomont, O. Ramdani, L. Parissi, P. Panheleux, N. Naghavi, C. Hubert, M. Ben-Farah, J.P. Fauvarque, J. Connolly, O. Roussel, P. Mogensen, E. Mahe, J.F. Guillemoles, D. Lincot, O. Kerrec, Thin Solid Films 480 (2005) 526.
[12] S. Jost, F. Hergert, R. Hock, J. Schulze, A. Kirbs, T. VoX, M. Purwins, Sol. Energy Mater. Sol. Cells 91 (2007) 1669.
[13] S. Jost, F. Hergert, R. Hock, J. Schulze, A. Kirbs, T. VoX, M. Purwins, M. Schmid, Sol. Energy Mater. Sol. Cells 91 (2007) 636.
[14] M. Paire, S. Delbos, J.Vidal, N. Naghavi, J.F. Guillemoles, Chalcogenide thin film Solar Cells, in Solar Cells Materials, Wiley, 2014.
[15] Z. Li kao, N. Naghavi, F. Erfurth, J.F. Guillemoles, I. Gerard, A. Etcheberry, J.L. Pelouard, S. Collin, G.Voorwinden, D. Lincot, Progress in Photovoltaics, 20(2012)582.
[16] M. Paire, L. Lombez, J.F. Guillemoles, D. Lincot, J. Appl. Phys., 108(2010)034907.
[17] R.N. Bhattacharya, J. Electrochem. Soc. 130 (1983) 2040.
[18] O. Savadogo, Solar Energy Materials and Solar Cells 52 (1998) 361-388, Chemically and electrochemically deposited thin films for solar energy materials.
[19] F. Chraibi, M. Fahoume, A. Ennaoui, J.L. Delplancke, Phys. Status Solidi A 186(2001) 373.

[20] Armin E. Zaghi , Marie Buffiere, Guy Brammertz, Maria Batuk, Nick Lenaers, Bas Kniknie, Joke Hadermann, Marc Meuris, Jef Poortmans, Jef Vleugels, aAdvanced Powder Technology 25 (2014) 1254–1261

[21] K. Darowicki , S. Krakowiak, P. Slepski, Electrochimica Acta 51 (2006) 2204–2208, Selection of measurement frequency in Mott–Schottky analysis of passive layer on nickel.

[22] L. Djellal, S. Omeiri, A. Bouguelia, M. Trari, Photoelectrochemical hydrogen-evolution over p-type chalcopyrite $CuInSe_2$, Journal of Alloys and Compounds 476 (2009) 584–589

[23] Sreekanth Mandati, Bulusu V. Sarada, Suhash R. Dey, Shrikant V. Joshi, Journal of Power Sources, 273 (2015) 149-157.

[24] Brandon K. Durant, B.A. Parkinson, Solar Energy Materials&Solar Cells144(2016)586–591.

[25] Zhou Cao, Sui Yang, Mang Wang, Xiaopan Huang, Hongxing Li, Jie Yi, Jianxin Zhong, Solar Energy 139 (2016) 29–35

[26] Sreekanth Mandati, Bulusu V. Sarada, Suhash R. Dey, Shrikant V. Joshi, Journal of Power Sources 273 (2015) 149-157.

[27] M. Sharon, an Introduction to the Physics and Electrochemistry of Semiconductors: Fundamentals and Applications, Published 2016 by John Wiley & Sons, Inc, DOI: 10.1002/9781119274360